UNCERTAINTY PROPAGATION IN ESTIMATION OF PARTIAL 3D VELOCITY

Nuno Gonçalves and Helder Araújo

Institute of Systems and Robotics - Coimbra
Dept. of Electrical and Computers Engineering
University of Coimbra
Pinhal de Marrocos - POLO II - 3030 Coimbra
PORTUGAL
email: {nunogon,helder}@isr.uc.pt

Keywords: uncertainty propagation, 3D velocity, rotation, translation, depth resolution

Abstract

This paper analyses two methods to compute the 3D velocity of a navigating stereo head in the depth (Z) direction. Both methods, which are function of the optical flow and disparity maps, are presented in two approaches: differential and discrete. All the expressions of both methods in both formulations are studied within the scope of uncertainty propagation. This provides a mean to point out the critical input variables for each method where special care in measurements should be taken. Different paths (translational, rotational and mixed) as well as different types of surfaces are compared.

1 Introduction

Motion estimation has been studied mainly within the framework of rigid body motion. However, in robotics literature it is easy to find the motion estimation problem also stated in a different way: the estimation of the time-to-impact (TTI) or time-to-collision.

This quantity yields the time needed to impact with the nearest obstacle if the motion remains unchanged. It can be computed with the expression:

$$TTI = \frac{Z}{V_Z} \tag{1}$$

where Z is the depth of the nearest obstacle and V_Z is the 3D motion of the vehicle in the depth (Z) direction. Given the depth information the problem becomes the estimation of V_Z.

In robotics applications it is very important to avoid the collision with obstacles and the TTI performs an important role in that matter. Physiological researchers [7] stated that in the human (and animal, in general) visual system the speed of self-motion can not be determined visually using only the optical flow pattern. TTI, however, can be directly measured from the optical flow. There is no general agreement if human uses or not this strategy in avoiding collisions.

Colombo [1] points out that often the TTI is confused with scaled depth (which considers only the translational motion). This approximation is reasonable when a narrow field of view is used but at the image periphery gross estimation errors should be expected. To avoid this model error, both translational and rotational components of rigid body motion should be considered.

In this paper we are interested in the computation of the denominator of expression 1, that is the 3D velocity of the navigating system in the Z direction. This velocity is a function of the rigid body translational and rotational velocities which are in general unknown. Two methods ([9, 5, 2, 4]) are presented to compute V_Z, using optical flow and disparity maps (which provide the depth information used both for V_Z and for TTI) in stereo sequences. Both methods are formulated in a differential and discrete ap-

proaches.

This paper analyses those methods within the scope of uncertainty propagation. Errors in the input variables used to compute V_Z will inevitably corrupt their results. Even very small errors in the optical flow and disparity information can produce a high level of uncertainty in the values of V_Z. This fact reduces the accuracy and the interest of such a computation (it also suggests that a high number of measurements have to be done) and that is why the quantification of the uncertainty if fundamental.

The aim of this work is to quantify the variance of the computed values for V_Z which provides a mean to point out the critical input variables in the methods. Those critical factors indicate which measurements should be carefully done.

In the next section the problem of motion estimation is stated and in the following two sections the differential and discrete approaches are presented. Section 5 derives the uncertainty propagation expressions for both methods (two approaches) and in section 6 some experiments are described and results are presented. Section 7 presents some conclusions of the work.

2 Motion Estimation

Before the description of the methods used to compute the 3D velocity, we shall first introduce the notations and geometry used throughout this paper.

In this paper a 3D point in space is designated by its coordinate vector $\mathbf{P} = [X\ Y\ Z]^T$ and the world coordinate system is coincident with the cyclopean coordinate system, that is, centred in the middle point between the optical centres of both cameras. The origins of the local camera coordinate systems are the optical centres at a distance *f* (focal length) of the image plane. Both cameras are parallel to each other separated by the baseline *b*. The flow induced in the image planes is represented by $v^l = (v^l_x, v^l_y)$ for the left image plane and by $v^r = (v^r_x, v^r_y)$ for the right image plane.

Figure 1 shows the geometry of the stereo vision system and the world coordinate system.

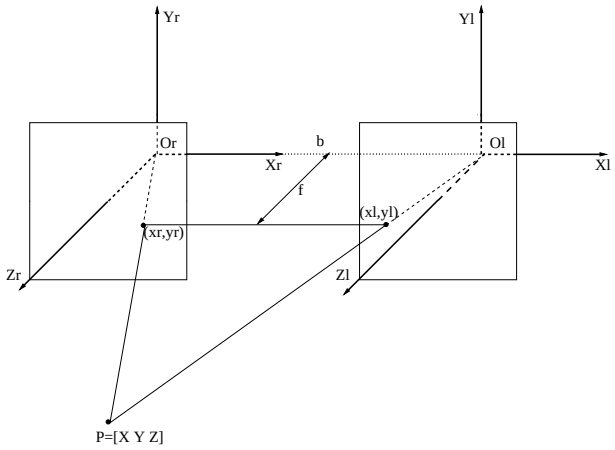

Figure 1: World and stereo coordinate system

The model used for the 3D total velocity of a point $\mathbf{P}$ in space is the rigid body motion. Let $\mathbf{V}$ be the total 3D velocity of the point $\mathbf{P}$. As any rigid body motion can be expressed by a translational component given by $\mathbf{t} = [t_X\ t_Y\ t_Z]^T$ and a rotational component given by $\mathbf{\Omega} = [\Omega_X\ \Omega_Y\ \Omega_Z]^T$ the 3D velocity is given by $\mathbf{V} = \mathbf{t} + \mathbf{\Omega} \times \mathbf{P}$.

Computing the components of the total 3D velocity $\mathbf{V}$, it is obtained the following expression:

$$\mathbf{V} = \begin{bmatrix} t_X + \Omega_Y Z - \Omega_Z Y \\ t_Y + \Omega_Z X - \Omega_X Z \\ t_Z + \Omega_X Y - \Omega_Y X \end{bmatrix} = \begin{bmatrix} V_X \\ V_Y \\ V_Z \end{bmatrix} = \begin{bmatrix} \dot{X} \\ \dot{Y} \\ \dot{Z} \end{bmatrix} \quad (2)$$

The third component of the 3D velocity - V_Z - is the velocity of the scene points in the direction of the optical axis which is the quantity to be estimated (providing a mean to compute the time-to-impact ($TTI = Z/V_Z$)).

Besides that, there are two possible approaches to the problem of V_Z estimation: differential and discrete. The two methods in both approaches are presented in the next sections.

3 Differential approach

In this section 3D motion estimation is considered from a differential standpoint. The correspondences across time are not known and the differential optical flow is available. Two methods to estimate the 3D

velocity in the Z direction - V_Z are presented. The details and proofs of those methods are available in [3, 2, 9, 5].

$\mathbf{V_Z}$ - Depth Constraint

The change in the depth of a point or rigid body over time is directly related to its velocity in 3D space. It can be used this principle to relate the velocity in the Z direction with depth.

The depth at instant t' of a point should be the depth at the instant t plus the displacement in the Z direction - V_Z. This relationship is given by the following expression, the linear Depth Change Constraint Equation - DCCE (first order Taylor series approximation):

$$V_Z = Z_t + Z_x \cdot v_x + Z_y \cdot v_y \tag{3}$$

where $Z(x, y, t)$ is the depth at a given time t, Z_x, Z_y and Z_t its spatial-temporal derivatives. v_x and v_y are the components of the optical flow.

$\mathbf{V_Z}$ - Binocular Flow Constraint

The second method to compute V_Z is based on the differences between the flows induced by the movement of a point in a stereo pair of images [9]. The parallel stereo system is again used and is considered to move rigidly with the scene.

Point $\mathbf{P}$ in figure 1, its projection in each image plane ((x_l, y_l, f) and (x_r, y_r, f)) and the optical centres (O_l and O_r) define two similar triangles, so that the following relationship can be written:

$$\frac{Z}{b} = \frac{Z - f}{b - (x^r - x^l)} \tag{4}$$

Now, computing the temporal derivative of the equation 4, it yields:

$$V_Z = -\frac{bf}{(x^r - x^l)^2} \cdot (v_x^r - v_x^l) = -\frac{Z^2}{bf} \Delta v_x \tag{5}$$

4 Discrete Formulation

This section presents the discrete versions of both methods to compute V_Z.

In the discrete formulation of DCCE and binocular flow methods the depth information is assumed to be available and so the disparity in time t and t' (d and d') are known. Feature correspondences are also available.

$\mathbf{V_Z}$ - Discrete DCCE

The DCCE equation in the discrete formulation is given by:

$$V_Z = Z_t + Z_x \Delta x + Z_y \Delta y \tag{6}$$

where $Z_t = Z(x, y, t') - Z(x, y, t)$.

In the discrete formulation of the DCCE equation, the image velocities were replaced by the finite differences of the point image coordinates.

$\mathbf{V_Z}$ Binocular Flow

The discrete binocular flow method equation is given by:

$$V_Z \approx -\frac{ZZ'}{bf} (\Delta x_r - \Delta x_l) \tag{7}$$

or, in a easier way to compute, after rearranging the terms:

$$V_Z \approx -\frac{ZZ'}{bf} (d' - d) \tag{8}$$

5 Uncertainty Propagation

Given the two models for V_Z, both in the differential and discrete approaches, it is important to analyse the uncertainty propagation in the equations due to uncertainty in the data inputs. As we shall see, it is possible to determine the critical independent variables that in presence of uncertainties affect the recovery of motion.

The first step is to define the independent variables for each expression:

$$\begin{cases} V_{Z_1}\left(Z_x, Z_y, Z_t, v_x, v_y\right) = Z_t + Z_x v_x + Z_y v_y \\ V_{Z_2}\left(Z, v_x^l, v_x^r\right) = -\frac{Z^2}{bf}\Delta v_x \\ V_{Z_3}\left(Z_x, Z_y, Z_t, x, y, x', y'\right) = Z_t + Z_x \Delta x + Z_y \Delta y \\ V_{Z_4}\left(Z, Z', d, d'\right) = -\frac{ZZ'}{bf}\left(d' - d\right) \end{cases} \tag{9}$$

where the geometric parameters are assumed to be known, that is, the baseline and the focal length.

Any noise in the values of the disparity maps, depth data, their temporal and spatial derivatives and in the binocular image flows affect the computation of V_Z.

To study the uncertainty propagation, the covariance matrix of an expression that depends on an input variable vector is computed. Let $\mathbf{F}$ be the function vector to be estimated and $\mathbf{S}$ the vector with the independent variables. Consider $\mathbf{S}$ a n-vector random variable and $\mathbf{F}$ a m-vector random variable function of the n-vector $\mathbf{S}$. Notice that the relation between $\mathbf{F}$ and $\mathbf{S}$ is nonlinear. If it is considered the mean point of the random variables and computed the first order approximation it can be written the covariance matrix Γ of the function vector $\mathbf{F}$ in the form [6]:

$$\Gamma = \frac{\partial \mathbf{F}}{\partial \mathbf{S}} \cdot \Lambda \cdot \frac{\partial \mathbf{F}}{\partial \mathbf{S}}^T \tag{10}$$

where Λ is the covariance matrix of the input variables $\mathbf{S}$. $\partial\mathbf{F}/\partial\mathbf{S}$ is the Jacobian matrix that maps vector $\mathbf{S}$ to $\mathbf{F}$.

It is assumed that all variables are affected by Gaussian random white noise with zero mean and standard deviation denoted by σ_i, where i denotes the variable. Also the noise in the variables is assumed to be independent so the covariance matrix for this input signal $\mathbf{S}$ is given by:

$$\Lambda_{jk} = \begin{cases} \sigma_{ii}^2 \longrightarrow \text{for j=k} \\ 0 \longrightarrow \text{for j} \neq \text{ k} \end{cases} \tag{11}$$

In this study the depth is computed from the disparity with $Z = bf/d$ and so the uncertainty analysis is within the scope of the disparity and optical flow (differential and/or discrete). The V_Z expressions depend on depth and depth spatial and temporal gradients. So, before analysing each equation, the uncertainty propagation in the depth is first derived.

$$\sigma_{ZZ}^2 = \frac{\partial Z}{\partial d} \cdot \sigma_{dd}^2 \cdot \frac{\partial Z}{\partial d} = \frac{Z^4}{\left(bf\right)^2} \cdot \sigma_{dd}^2 \tag{12}$$

For the gradients of depth in relation to the variable i ($i \in \{x, y, t\}$) we have:

$$Z_i = \frac{\partial}{\partial i}\left(\frac{bf}{d}\right) = -\frac{bf}{d^2} \cdot d_i \tag{13}$$

so that

$$\sigma_{Z_i Z_i}^2 = \begin{bmatrix} \frac{\partial Z_i}{\partial d} & \frac{\partial Z_i}{\partial d_i} \end{bmatrix} \cdot \begin{bmatrix} \sigma_{dd}^2 & 0 \\ 0 & \sigma_{d_i d_i}^2 \end{bmatrix} \cdot \begin{bmatrix} \frac{\partial Z_i}{\partial d} \\ \\ \frac{\partial Z_i}{\partial d_i} \end{bmatrix} \tag{14}$$

The depth covariance expression becomes:

$$\sigma_{Z_i Z_i}^2 = \left(\frac{2bf}{d^3} d_i\right)^2 \cdot \sigma_{dd}^2 + \left(\frac{bf}{d^2}\right)^2 \cdot \sigma_{d_i d_i}^2 \tag{15}$$

It is now possible to concentrate the attention in the expressions of V_Z for both the DCCE and DV methods.

5.1 Depth Constraint - Differential

For the first expression it yields $\mathbf{F_1} = [V_Z]$ and $\mathbf{S_1} = [Z_x\ Z_y\ Z_t\ v_x\ v_y]^T$.

The covariance matrix for this input signal $\mathbf{S_1}$ is given by:

$$\Lambda_1 = \begin{bmatrix} \sigma_{Z_x Z_x}^2 & & \cdots & & 0 \\ & \sigma_{Z_y Z_y}^2 & & & \\ \vdots & & \sigma_{Z_t Z_t}^2 & & \vdots \\ & & & \sigma_{v_x v_x}^2 & \\ 0 & & \cdots & & \sigma_{v_y v_y}^2 \end{bmatrix} \tag{16}$$

To compute the covariance matrix of the function vector, equation 10 is used. It yields:

$$\Gamma_1 = \begin{bmatrix} v_x & v_y & 1 & Z_x & Z_y \end{bmatrix} \Lambda_1 \begin{bmatrix} v_x \\ v_y \\ 1 \\ Z_x \\ Z_y \end{bmatrix} \quad (17)$$

The resulting covariance matrix is a 1×1 matrix given by the expression:

$$\Gamma_1 = \sigma^2_{Z_x Z_x} v_x^2 + \sigma^2_{Z_y Z_y} v_y^2 + \sigma^2_{Z_t Z_t} + \sigma^2_{v_x v_x} Z_x^2 + \sigma^2_{v_y v_y} Z_y^2 \quad (18)$$

showing the dependencies on the variances of Z_i ($i \in \{x, y, t\}$). Substituting equations 13 and 15 in equation 18 it yields:

$$\Gamma_1 = \sigma^2_{V_Z V_Z,1} = \left(2\frac{bf}{d^3}\right)^2 \left(d_x^2 v_x^2 + d_y^2 v_y^2 + d_t^2\right) \sigma^2_{dd} + \\ + \left(\frac{bf}{d^2}\right)^2 \cdot \left(v_x^2 \sigma^2_{d_x d_x} + v_y^2 \sigma^2_{d_y d_y} + \sigma^2_{d_t d_t}\right) + \\ + \left(\frac{bf}{d^2}\right)^2 \cdot \left(d_x^2 \sigma^2_{v_x v_x} + d_y^2 \sigma^2_{v_y v_y}\right) \quad (19)$$

5.2 Binocular Flow Constraint - Differential

Using a similar reasoning for the second method:

$$\mathbf{S_2} = \begin{bmatrix} Z \\ v_x^l \\ v_x^r \end{bmatrix} \quad (20)$$

$$\Lambda_2 = \begin{bmatrix} \sigma^2_{ZZ} & 0 & 0 \\ 0 & \sigma^2_{v_x^l v_x^l} & 0 \\ 0 & 0 & \sigma^2_{v_x^r v_x^r} \end{bmatrix} \quad (21)$$

and the Jacobian matrix is:

$$\frac{\partial \mathbf{F_2}}{\partial \mathbf{S_2}} = \begin{bmatrix} -2\frac{Z}{bf}\Delta v_x & -\frac{Z^2}{bf} & \frac{Z^2}{bf} \end{bmatrix} \quad (22)$$

The covariance matrix of the function vector, after arranging the terms, is then:

$$\Gamma_2 = 4V_Z \sigma^2_{ZZ} + \frac{Z^4}{(bf)^2}\left(\sigma^2_{v_x^l v_x^l} + \sigma^2_{v_x^r v_x^r}\right) \quad (23)$$

and substituting equation 15 in equation 23 it is obtained:

$$\Gamma_2 = \sigma^2_{V_Z V_Z,2} = \frac{(2bf)^2}{d^6}(\Delta v_x)^2 \sigma^2_{dd} + \\ + \frac{(bf)^2}{d^4}\left(\sigma^2_{v_x^l v_x^l} + \sigma^2_{v_x^r v_x^r}\right) \quad (24)$$

5.3 Depth Constraint - Discrete

In this case the independent variables vector $\mathbf{S}$ is given by:

$$\mathbf{S_3} = \begin{bmatrix} Z_x & Z_y & Z_t & x & y & x' & y' \end{bmatrix}^T \quad (25)$$

The Jacobian matrix is straightforward in this function. The covariance matrix, dependent on the depth, yields:

$$\Gamma_3 = \left(\frac{\partial \mathbf{F_3}}{\partial \mathbf{S_3}}\right)^T \Lambda_3 \left(\frac{\partial \mathbf{F_3}}{\partial \mathbf{S_3}}\right) = \sigma^2_{Z_x Z_x}(x' - x)^2 + \\ + \sigma^2_{Z_y Z_y}(y' - y)^2 + \sigma^2_{Z_t Z_t} + \left(\sigma^2_{xx} + \sigma^2_{x'x'}\right) Z_x^2 + \\ + \left(\sigma^2_{yy} + \sigma^2_{y'y'}\right) Z_y^2 \quad (26)$$

and substituting equations 13 and 15 in equation 26 it is obtained:

$$\Gamma_3 = \sigma^2_{V_Z V_Z,3} = \\ = \left(2\frac{bf}{d^3}\right)^2 \left(d_x^2 (\Delta x)^2 + d_y^2 (\Delta y)^2 + d_t^2\right) \sigma^2_{dd} + \\ + \left(\frac{bf}{d^2}\right)^2 \cdot \Big[(\Delta x)^2 \cdot \sigma^2_{d_x d_x} + (\Delta y)^2 \cdot \sigma^2_{d_y d_y} + \sigma^2_{d_t d_t} + \\ + d_x^2 \left(\sigma^2_{xx} + \sigma^2_{x'x'}\right) + d_y^2 \left(\sigma^2_{yy} + \sigma^2_{y'y'}\right) \Big] \quad (27)$$

5.4 Binocular Flow Constraint - Discrete

Using the same reasoning, the independent variables vector for the discrete binocular flow method yields:

$$\mathbf{S_4} = \begin{bmatrix} Z & Z' & d & d' \end{bmatrix}^T \quad (28)$$

Calculating the jacobian matrix and substituting it in the first order approximation of the covariance matrix of $\mathbf{F_4}$, it yields:

$$\Gamma_4 = \left(1 - \frac{d}{d'}\right)^2 \sigma_{ZZ}^2 + \left(\frac{d'}{d} - 1\right)^2 \sigma_{Z'Z'}^2 + \\ + \frac{Z^2 Z'^2}{(bf)^2}\left(\sigma_{dd}^2 + \sigma_{d'd'}^2\right) \quad (29)$$

and putting together equation 15 and equation 29 it is obtained:

$$\Gamma_4 = \sigma_{V_Z V_Z,4}^2 = \left(\frac{bf}{d^2}\right)^2 \cdot \sigma_{dd}^2 + \left(\frac{bf}{d'^2}\right)^2 \cdot \sigma_{d'd'}^2 \quad (30)$$

5.5 Resolution of Depth Data

The uncertainty caused by random noise in the input variables strongly affects the accuracy of the estimation of V_Z. Besides that, the finite resolution of the disparity maps can be one important source of error and affects even more the V_Z estimation accuracy. Figure 2 shows how the resolution of the disparity can produce uncertainty in the position of a 3D point, mainly in the depth coordinate.

The software used in our study to obtain the disparity fields has a finite resolution of $1/16$ of pixel. So, some changes in the real depth of a point do not produce any change in the disparity and since depth is inversely proportional to the disparity its value is calculated with decreasing resolution as the value of the depth itself increases.

Let Δd be the minimum change in disparity. Then the minimum change in depth that produce changes in disparity is:

$$Z = \frac{bf}{d} \longrightarrow \Delta Z = -\frac{1}{1 + \frac{d}{\Delta d}} \cdot \frac{bf}{d} = -\frac{1}{1 + \frac{d}{\Delta d}} \cdot Z \quad (31)$$

Equation 31 indicates that for near objects small changes in depth cause high changes in the disparity and for distant objects the minimum change in depth that produce changes in the disparity is very high.

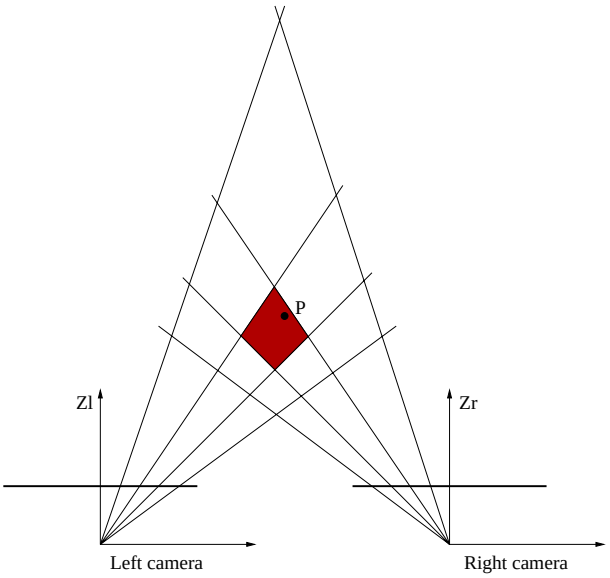

Figure 2: Effect of finite resolution of disparity maps in depth

So, let us consider a realistic situation: $b = 130$mm, $f = 5$mm, $\Delta d = 1/16$px and the pixel width $pw = 0.012$mm.

In that particular case it is obtained, for example:

- $d = 1 \longrightarrow Z = 54167 \longrightarrow \Delta Z = -3186\ mm$
- $d = 5 \longrightarrow Z = 10833 \longrightarrow \Delta Z = -133.7\ mm$
- $d = 10 \longrightarrow Z = 5417 \longrightarrow \Delta Z = -33.7\ mm$
- $d = 20 \longrightarrow Z = 2708 \longrightarrow \Delta Z = -8.4\ mm$
- $d = 50 \longrightarrow Z = 1083 \longrightarrow \Delta Z = -1.4\ mm$

However, if the resolution lowers to $1/4px$, for the same case, it yields:

- $d = 1 \longrightarrow Z = 54167 \longrightarrow \Delta Z = -10833\ mm$
- $d = 5 \longrightarrow Z = 10833 \longrightarrow \Delta Z = -515.9\ mm$
- $d = 10 \longrightarrow Z = 5417 \longrightarrow \Delta Z = -132.1\ mm$
- $d = 20 \longrightarrow Z = 2708 \longrightarrow \Delta Z = -33.4\ mm$
- $d = 50 \longrightarrow Z = 1083 \longrightarrow \Delta Z = -5.4\ mm$

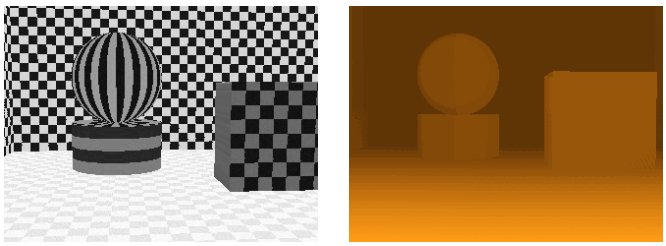

(a) Left image (b) Disparity

Figure 3: Intensity images and disparity field for synthetic world

It can be seen that the low resolution in disparity/depth data can produce large errors with increasing distance to the optical centre of the camera. This fact will produce significant errors in the computation of depth field gradients mainly for small motion between two consecutive frames. This also means that it will be difficult to recover motion for distant points (unless high resolution disparity is used).

The perturbation caused by rounding/quantization error (limited resolution) is given by the following equation [8]:

$$\sigma_{dd}^2 = \frac{step^2}{12} \tag{32}$$

where $step$ is the minimum increment due to finite resolution.

6 Experiments and Results

To analyse quantitatively the uncertainty equations 19, 24, 27 and 30, it was constructed a synthetic world composed by several objects: front and lateral walls, ground plane, a box on the ground, a cylinder and a sphere. Figure 3 shows the left image of a synthetic stereo pair and the corresponding disparity map.

This world was projected into two equal cameras mounted in a virtual navigation robot with baseline $130mm$, focal length $5.0mm$, square pixels width of $0.012mm$. The virtual robot performed several paths (translational, rotational and mixed paths) and the data stored includes: left and right images, disparity in high resolution (map of floats) and continuous and discrete image velocities.

The uncertainty equations represent the variance of the estimation of V_Z in each point. Given the disparity maps, as well as their spatial and temporal gradients and the continuous and discrete velocities, the uncertainty for each point using equations 19, 24, 27 and 30 can be computed as function of the variance of the input variables.

For that purpose the following assumptions are made: the variance of the differential and discrete image velocities are equal for both x and y coordinates ($\sigma_{vv}^2 = \sigma_{v_x^l v_x^l}^2 = \sigma_{v_y^l v_y^l}^2 = \sigma_{v_x^r v_x^r}^2 = \sigma_{v_y^r v_y^r}^2$) and the same for the discrete velocities, and for the gradients of the disparity $\sigma_{d_i d_i}^2 = 0.5\sigma_{dd}^2$ since the derivatives of the disparity maps are approximated by a finite differences equation (for ex., $d_t(x,y,t) \approx 0.5 \cdot d(x,y,t+1) - 0.5 \cdot d(x,y,t-1)$).

The uncertainty propagation equation are then given by:

$$\Gamma_j = Coef_{jd} \cdot \sigma_{dd}^2 + Coef_{jv} \cdot \sigma_{vv}^2 \tag{33}$$

where $j \in \{1,2,3,4\}$ and represent one of the methods (DCCE/DIF, DV/DIF, DCCE/DISC and DV/DISC respectively). $Coef_{jd}$ and $Coef_{jv}$ are the weights of the disparity and velocities random noises.

From the variance equations of all expressions and from equation 31 it is clear that the distance of a point to the optical centre is one of the most important factors to the uncertainty value (variance). To observe this sentence, figure 4 plots the variance value for equation 19 where darker points represent values with low variance and lighter points have higher variance (saturation for values equal and above $3000mm^2$). It can be seen that farther objects have higher variances. The map for the uncertainty equations Γ_2 to Γ_4 are not presented since they are very close to one another.

Table 1 presents some values for the uncertainty coefficients. Two points from four objects were chosen: (G)round, (B)ox A, (S)phere and (W)all. The points are sorted in increasing order of its depth.

Regarding the values reported in table 1 it can be observed that, as was expected, for farther objects the

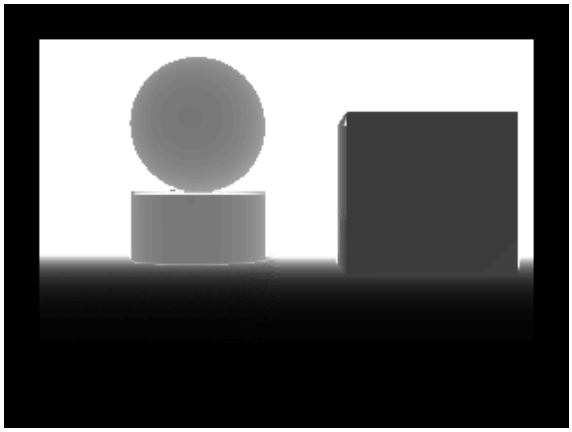

Figure 4: Variance map for Γ_1. Lighter point have higher variance. It was used $\sigma^2_{dd} = \sigma^2_{vv} = 0.0052$ calculated from equation 32, corresponding to a resolution of $1/4px$.

		Γ_1	Γ_2	Γ_3	Γ_4
G	$Coef_{i1}$	13216	81.2	13275	10774
	$Coef_{i2}$	256.2	11993	256.2	–
G	$Coef_{i1}$	63364	198.0	63517	57711
	$Coef_{i2}$	1299	61532	1299	–
B	$Coef_{i1}$	52768	133.8	52825	48038
	$Coef_{i2}$	1.6	51563	1.6	–
B	$Coef_{i1}$	57902	100.3	57958	51740
	$Coef_{i2}$	1218	56170	1218	–
S	$Coef_{i1}$	94444	312.7	94516	87223
	$Coef_{i2}$	0.3	94050	0.3	–
S	$Coef_{i1}$	108960	308.2	109100	101237
	$Coef_{i2}$	85.7	108375	85.7	–
W	$Coef_{i1}$	392981	485.6	393179	373989
	$Coef_{i2}$	1.4	392359	1.4	–
W	$Coef_{i1}$	370668	576.8	370843	350382
	$Coef_{i2}$	1.4	369942	1.4	–

Table 1: Uncertainty coefficients for points at different depths

variance of the V_Z estimation values is higher. It can also be noticed that the DCCE method is much more sensitive to the uncertainty in the disparity map than to the uncertainty in the velocities. The binocular flow method (DV), however, in the differential approach is sensitive almost only to the uncertainty in velocities and, in the discrete approach, to the uncertainty in the disparity. Furthermore, the coefficients $Coef_{11}$, $Coef_{31}$, $Coef_{41}$ (dependence on the disparity) and $Coef_{22}$ (dependence on the velocities) present values very close to each other. This suggests that when the uncertainty in the disparity is similar to the uncertainty in the velocities, the uncertainty of V_Z estimation values are very similar for both methods in both formulations.

To see more explicitly the relation between the uncertainty coefficients and the depth of the points used to compute V_Z, figure 5 plots these uncertainty coefficients when a sphere is moved from 2.5 meters to 5 meters with the same motion conditions.

The depth, however, isn't the only variable that influences the uncertainty in the V_Z estimation. It is known that the path also plays an important role in the accuracy of the V_Z estimated. We concluded in [2, 3] that for pure rotational paths the V_Z estimation accuracy is poor. Furthermore, the amplitude of the velocities also affects the results. To observe these effects, figure 6 plots all uncertainty coefficients when the velocities are multiplied by a factor of 2, 4, 8, 16 and 32, in three paths: (A) pure translation through optical axis direction, (B) pure rotation over the vertical axis and (C) translation through all axis and rotation over vertical and horizontal axis.

Regarding figure 6 it can be observed that for the DCCE method, in both formulations, the first uncertainty coefficients ($Coef_{11}$ and $Coef_{31}$) grow up with the increase of the velocities in the rotational paths and don't present variations in translational and mixed paths. For the coefficients dependent on the uncertainty in the velocities ($Coef_{12}$ and $Coef_{32}$), it can be seen that they are around their mean value and don't increase or decrease. For the differential approach of the binocular flow method the coefficient $Coef_{21}$ increases for all paths and presents only slightly changes in $Coef_{22}$. In the discrete formulation, however, it is observed that there

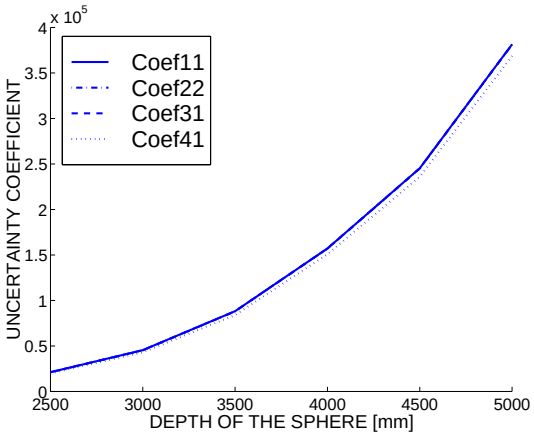

(a) $Coef_{11}$, $Coef_{22}$, $Coef_{31}$ and $Coef_{41}$

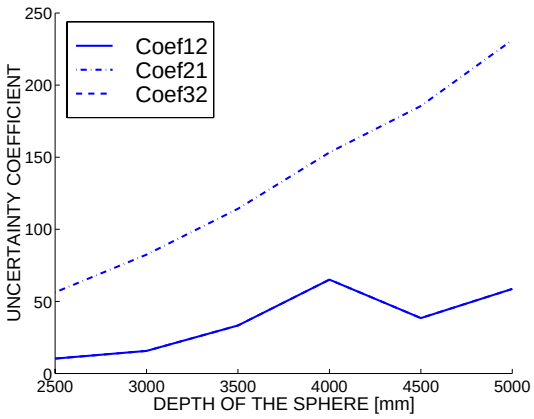

(b) $Coef_{12}$, $Coef_{21}$ and $Coef_{32}$

Figure 5: Uncertainty coefficients - depth effect.

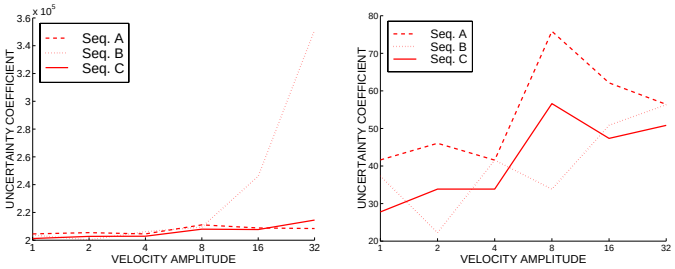

(a) $Coef_{11}$ (b) $Coef_{12}$

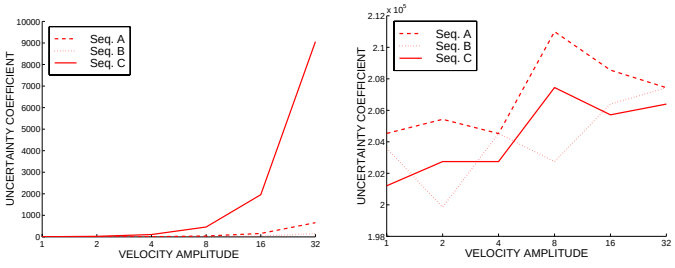

(c) $Coef_{21}$ (d) $Coef_{22}$

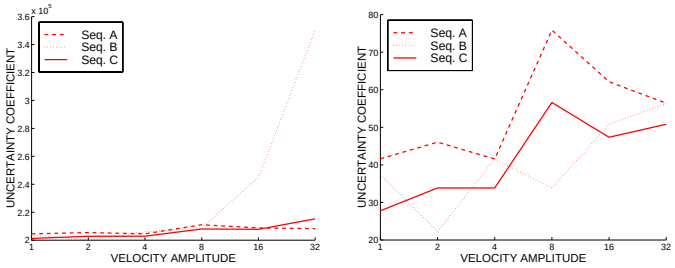

(e) $Coef_{31}$ (f) $Coef_{32}$

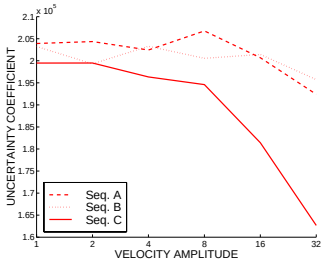

(g) $Coef_{41}$

Figure 6: Uncertainty coefficients - effect of the amplitude of velocities in three paths.

is a decrease of the uncertainty coefficient $Coef_{41}$.

It is also noticed that the rotational path presents higher values of uncertainty for almost all coefficients and velocities.

7 Conclusions

In this paper the uncertainty propagation expressions of the third component of 3D velocity estimation are derived. Those expressions were written as function of the uncertainty on the disparity map and the uncertainty on the velocities (continuous and discrete).

From the analysis of the expressions and the results plotted it is possible to conclude that, for the DCCE method, both in the differential and in the discrete formulations, the critical factor is the disparity. There is an increasing tendency of the uncertainty coefficients when the velocities themselves increase.

For the DV method, however, the two formulations have distinct behaviors. For the differential one, the critical factor is the uncertainty on velocities and for the discrete one the critical factor is the uncertainty on the disparity. The former approach presents an increasing of the uncertainty coefficients when velocities grow up and the discrete approach presents a decreasing in that situation.

In the DCCE method as well as in the DV method, in both approaches, the coefficients of the critical factors were ever much bigger than the other ones. The difference is between one and five orders of magnitude.

It was also observed that the 3D point depth relatively to the cameras is very important to the uncertainty coefficients. Those coefficients grow up in a high power (between 2 and 4) of the depth coordinate, so farther objects have higher uncertainty which suggests that the V_Z is more accurate when closer points are used.

Furthermore, some paths were compared and it was observed that in rotational paths the uncertainty coefficients were bigger than in translational and even mixed paths. This suggests that rotational motion is more difficult to estimate.

References

[1] C. Colombo and A. Del Bimbo. Generalized Bounds for Time to Collision from First-Order Image Motion. In *7th IEEE International Conference on Computer Vision*, pages 220–226, Corfu, Greece, September 1999. IEEE.

[2] N. Gonçalves. Estimação de movimento em sequências de imagens estéreo - comparação de dois métodos. Master's thesis, Department of Electrical and Computers Engineering of the Faculty of Science and Technology of the University of Coimbra, 2002.

[3] N. Gonçalves and H. Araújo. Analysis of two methods for the estimation of partial 3d velocity. In *Proc. of the 9th International Symposium on Intelligent Robotic Systems*, Toulouse, France, 2001.

[4] N. Gonçalves and H. Araújo. Estimation of 3d motion from stereo images - differential and discrete formulations. In *Proc. of the 16th International Conference on Pattern Recognition*, August 2002.

[5] M. Harville, A. Rahimi, T. Darrell, G. Gordon, and J. Woodfill. 3d pose tracking with linear depth and brightness constraints. In *Proc. IEEE International Conference on Computer Vision*, Corfu, Greece, 1999.

[6] K. Kanatani. *Statistical Optimization for Geometric Computation: Theory and Practice*. Machine Intelligence and Pattern Recognition - vol. 18. North-Holland - Elsevier, 1996.

[7] S. Palmer. *Vision Science: Photons to Phenomenology*. MIT Press, 1999.

[8] K. Shanmugan. *Digital and analog communication systems*. John Wiley & Sons, 1979.

[9] A. M. Waxman and J. H. Duncan. Binocular image flows: Steps towards stereo - motion fusion. *IEEE Trans. on Pattern Analysis and Machine Intelligence*, 8(6):715–729, Nov. 1986.